# Symmetrical Quasi-Absorptive RF Bandpass Filters

Roberto Gómez-García<sup>®</sup>, *Senior Member, IEEE*, José-María Muñoz-Ferreras<sup>®</sup>, *Member, IEEE*, and Dimitra Psychogiou<sup>®</sup>, *Member, IEEE* 

Abstract—A type of symmetrical RF bandpass filters (BPFs) with quasi-absorptive functionality are presented. They are composed of a bandpass section that is loaded at its input/output ports with nearly complementary resistively terminated bandstop sections. In this manner, the input-signal energy that is not transmitted by the bandpass section is dissipated by the loading resistors of the bandstop sections to attain the quasireflectionless behavior. The theoretical analysis of the first-order symmetrical quasi-absorptive BPF stage is detailed. In addition, synthesis examples of higher attenuation and sharper rejection designs based on in-series-cascade arrangements, higher order realizations, and cross-coupling techniques are illustrated. A coupling-matrix-level loss analysis of the devised symmetrical quasi-reflectionless BPF configuration for uniform and nonuniform quality-factor (0) distribution is also carried out. Furthermore, for experimental validation, 2.5-GHz microstrip BPF demonstrators consisting of an in-band linear-phase twostage in-series-cascade circuit and a second-order prototype are manufactured and characterized.

Index Terms—Absorptive filter, bandpass filter (BPF), circulator, coupling matrix, isolator, microstrip filter, microwave filter, planar filter, quasi-elliptic filter, reflectionless filter, RF filter.

#### I. INTRODUCTION

ITH the advent of new wireless communications systems (e.g., 5G) aimed at providing the users with multiple services simultaneously, highly advanced RF electronics need to be developed [1], [2]. In the case of high-frequency bandpass filters (BPFs), such necessity usually refers to the realization of very efficient filtering actions for highly robust signal-band selection processes. Nevertheless, other performance requisites, such as: 1) transfer-function adaptivity—in terms of center frequency, bandwidth, and commutation to bandstop filtering modes for receiver protection; 2) multiband functionality; 3) tunable notch embedding in passband regions for dynamic in-band RF-interference mitigation; and 4) differential-mode operation for noise and common-mode suppression, are acquiring a paramount importance [3]–[6].

Manuscript received January 1, 2018; revised May 27, 2018 and September 14, 2018; accepted December 22, 2018. Date of publication February 8, 2019; date of current version April 3, 2019. This work was supported in part by the Spanish Ministry of Economy and Competitiveness under Project TEC2017-82398-R and in part by the National Science Foundation under Award 1731956. (Corresponding author: Roberto Gómez-García.)

R. Gómez-García and J.-M. Muñoz-Ferreras are with the Department of Signal Theory and Communications, Polytechnic School, University of Alcalá, 28871 Alcalá de Henares, Spain (e-mail: roberto.gomez.garcia@ieee.org; jm.munoz@uah.es).

D. Psychogiou is with the Department of Electrical, Computer, and Energy Engineering, University of Colorado Boulder, Boulder, CO 80309 USA (e-mail: dimitra.psychogiou@colorado.edu).

Color versions of one or more of the figures in this paper are available online at http://ieeexplore.ieee.org.

Digital Object Identifier 10.1109/TMTT.2019.2895531

Absorptive or reflectionless RF BPFs have been recently explored for a more robust operation of the entire RF chain. Contrary to most of RF BPF topologies available in the technical literature, these filters dissipate inside themselves the nontransmitted input-signal energy in the stopband regions instead of reflecting it back to the source. As a result, undesired power reflections that can perceptibly deteriorate the behavior of adjacent RF active stages (e.g., damaging of coherent source generators, instability issues in low-noise amplifiers, or creation of additional unwanted intermodulation products through remixing with the local oscillator in frequency converters) are avoided [7]. This alleviates the need for nonreciprocal components (e.g., isolators and circulators) in the complete RF system to circumvent this problem, which are usually bulky and difficult to integrate [8].

Despite a plurality of absorptive bandstop filters with staticand frequency-reconfigurable characteristics for a variety of RF technologies have been reported (see [9], [10]), much fewer reflectionless BPF architectures have been conceived. Some exponents to be remarked upon are those in [11]-[14] that exhibit some limitations. For example, the use of power directional couplers in [11] makes the filter difficult to tune and increases its physical size. In [12] and [13], remarkable selectivity is obtained for the first-order symmetrical fully reflectionless BPF section that is composed of six resonators arranged in a transversal two-path structure. However, its synthe sized transfer function cannot be arbitrarily designed since the transmission zeros and bandwidth cannot be controlled independently. Besides, it requires unrealizable characteristicimpedance values in its transmission-line-based version for moderate-to-narrowband designs. On the other hand, the BPF approach in [14] is restricted to low-selectivity designs. In an authors' previous work, a new family of fully absorptive adaptive RF filters based on complementary duplexers was proposed [15]. Nevertheless, they only feature the reflectionless behavior at their input terminal (i.e., not at both ports) and their experimental demonstration was limited to first-order implementations and their in-series cascades. Furthermore, the realization of linear-phase/flat-group-delay-type reflectionless BPFs was not addressed.

In this paper, a generalization of the filter concept in [15] to design symmetrical quasi-absorptive BPFs is presented. This means that the quasi-reflectionless behavior is attained in these BPFs at their two ports and not only at their input access in order to eliminate RF-power reflections at their two terminals. The organization of the rest of this paper is as follows: the theoretical foundations of the conceived symmetrical quasi-reflectionless BPF and illustrative synthesis examples are described in Section II. For practical verification purposes,

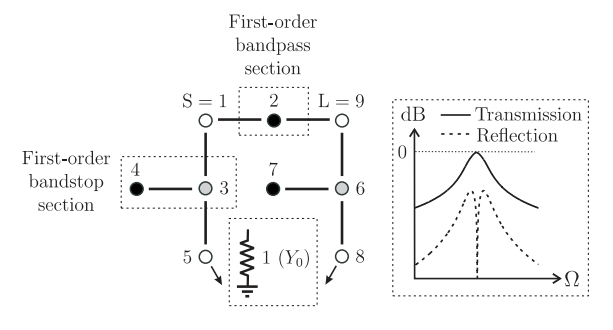


Fig. 1. Normalized coupling-routing diagram and operating principle of the proposed first-order symmetrical quasi-absorptive BPF [black circles: resonating nodes; gray circles: zero-susceptance NRNs; white circles: unitary source (S), load (L), and loading resistors—i.e., nodes 5 and 8 correspond to the one-port grounded-unitary-resistor element represented inside the dotted-line box; continuous lines: couplings;  $\Omega$ : normalized frequency; and  $Y_0 = 1/Z_0$ : reference admittance for admittance normalization]. Note that  $M_{1,2} = M_{2,9}$ .  $M_{1,3} = M_{6,9}$ ,  $M_{3,4} = M_{6,7}$ ,  $M_{3,5} = M_{6,8}$ , and  $M_{4,4} = M_{7,7}$  are satisfied in this two-port filtering network as a result of its symmetry property.

measured results of two manufactured microstrip prototypes centered at 2.5 GHz are shown in Section III. Finally, the main concluding remarks of this paper are set out in Section IV.

#### II. THEORETICAL FOUNDATIONS

The theoretical principles of the devised symmetrical quasiabsorptive BPF are described in this section. First, the analysis of the first-order stage of this filter principle is detailed. Subsequently, synthesis examples of higher attenuation and sharper rejection designs based on multistage schemes, higher order arrangements, and cross-coupling techniques are presented. Finally, the influence of the loss of the resonating nodes in the engineered symmetrical quasi-reflectionless BPF is analyzed and its comparison with relevant prior art reflectionless BPF configurations is also carried out.

#### A. First-Order Stage

The normalized coupling-routing diagram of the proposed first-order symmetrical quasi-absorptive BPF is shown in Fig. 1. It consists of a direct input-to-output bandpass section, in which the input/output ports are loaded with bandstop sections that are ended in a reference-impedance resistor. Thus, it comprises a total of three resonating nodes. Under certain design conditions, these resistors can absorb most of the input-signal energy that is not transmitted by the overall filter. As a result, a quasi-reflectionless behavior can be obtained.

The theoretical formulas for the normalized-to- $Y_0$  even- and odd-mode admittances of the symmetrical coupling-routing diagram in Fig. 1,  $Y_e(\Omega)$  and  $Y_o(\Omega)$ , respectively, are given by

$$Y_e(\Omega) = \frac{2M_{1,2}^2}{Y_R(\Omega)} + \frac{M_{1,3}^2 Y_R(\Omega)}{M_{3,4}^2 + M_{3,5}^2 Y_R(\Omega)}$$
(1)

$$Y_o(\Omega) = \frac{M_{1,3}^2 Y_R(\Omega)}{M_{3,4}^2 + M_{3,5}^2 Y_R(\Omega)}$$
 (2)

where  $\Omega \in [-\infty, +\infty]$  represents the normalized frequency variable,  $M_{i,j}$  (i, j = 1, 2, ..., 9) are coupling-matrix coefficients (i.e., admittance-inversion constants) [16], and  $Y_R(\Omega) = j\Omega$  corresponds to the normalized admittance

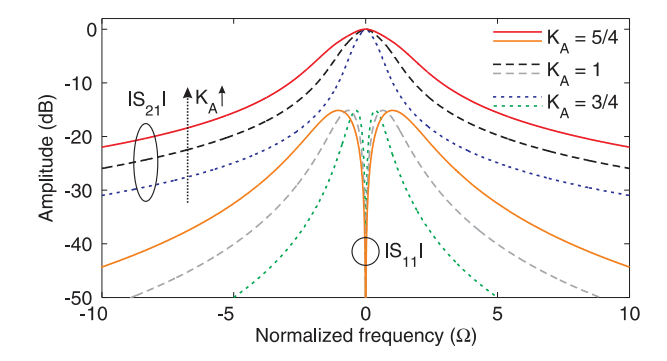


Fig. 2. Theoretical power transmission ( $|S_{21}| = |S_{12}|$ ) and reflection ( $|S_{11}| = |S_{22}|$ ) parameters of ideally synthesized examples for the first-order symmetrical quasi-absorptive BPF in Fig. 1.

associated with all resonating nodes that are synchronously tuned at  $\Omega = 0$  (i.e.,  $M_{2,2} = M_{4,4} = M_{7,7} = 0$ ).

From (1) and (2), it can be verified that the condition  $Y_e(\Omega)Y_o(\Omega) = 1$  cannot be satisfied for the entire normalized frequency range—see in the Appendix the corresponding theoretical demonstration. Hence, a fully absorptive behavior at any frequency is not feasible in the symmetrical BPF architecture in Fig. 1, [11]–[13]. Nevertheless, it has been observed that a quasi-reflectionless behavior is achieved if the following design relationships are fulfilled:

$$M_{1,2}^2 = K_A^2$$
  $M_{1,3}^2 = M_{3,5}^2 = K_B^2$   $M_{3,4}^2 = K_C^2 = K_A^2 K_B^2$  (3)

which lead—with (1) and (2)—to the following analytical expressions for the power transmission and reflection parameters of the filter scheme in Fig. 1,  $S_{21}(\Omega)$  and  $S_{11}(\Omega)$ , respectively,

$$S_{21}(\Omega) \equiv S_{12}(\Omega)$$

$$= \frac{Y_o(\Omega) - Y_e(\Omega)}{(1 + Y_e(\Omega))(1 + Y_o(\Omega))}$$

$$= -\frac{(1 + p)^2}{2(p + \frac{1}{2})(p + \frac{3}{4} + j\frac{\sqrt{7}}{4})(p + \frac{3}{4} - j\frac{\sqrt{7}}{4})}$$

$$S_{11}(\Omega) \equiv S_{22}(\Omega)$$

$$= \frac{1 - Y_e(\Omega)Y_o(\Omega)}{(1 + Y_e(\Omega))(1 + Y_o(\Omega))}$$

$$= -\frac{p}{4(p + \frac{1}{2})(p + \frac{3}{4} + j\frac{\sqrt{7}}{4})(p + \frac{3}{4} - j\frac{\sqrt{7}}{4})}$$
(5)

where  $p = j\Omega/K_A^2$ . Note that (4) and (5) do not depend on the  $K_B$  coefficient so that they are fully determined by  $K_A$ .

For illustration purposes, several examples of the theoretical power transmission and reflection responses in (4) and (5) associated with the first-order symmetrical BPF network in Fig. 1 are depicted in Fig. 2. As shown, a bandpass-type transfer function and a quasi-absorptive behavior are obtained in all cases with a maximum power reflection level of -15.15 dB. Furthermore, lower  $K_A$  values result in narrower passband widths while maintaining the same type of frequency variation profile for the power transmission and reflection parameters.

## B. Multistage, High-Order, and Sharp-Rejection Designs

High-stopband-attenuation and sharp-rejection bandpass filtering transfer functions for the devised symmetrical

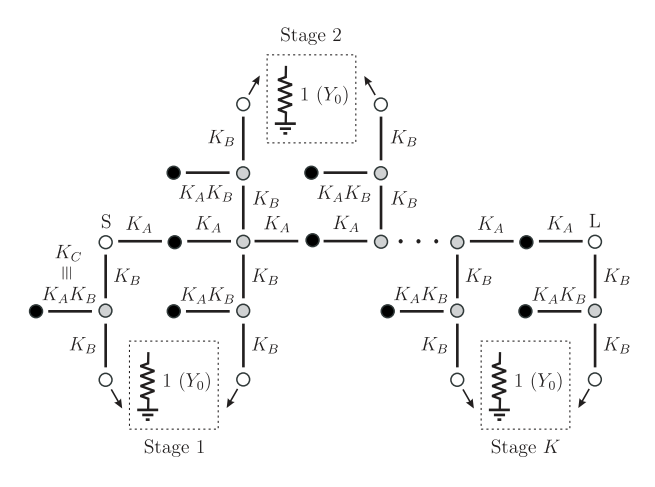


Fig. 3. Normalized coupling-routing diagram of the multistage in-series-cascade quasi-absorptive BPF [black circles: resonating nodes; gray circles: zero-susceptance NRNs; white circles: unitary source (S), load (L), and loading resistors; continuous lines: couplings; and  $Y_0 = 1/Z_0$ : reference admittance for admittance normalization].

quasi-absorptive BPF concept can be realized. To this aim, different RF design strategies can be exploited as described below.

As a first technique, multiple replicas of the first-order stage in Fig. 1 can be directly cascaded in series. This is illustrated in Fig. 3 for a K-stage arrangement. Note that due to the quasi-reflectionless behavior of its building firstorder stage, such characteristic is preserved in the overall BPF and its power transmission parameter satisfies  $S_{21}^{\rm casc}(\Omega) \approx$  $[S_{21}(\Omega)]^K$ —where  $S_{21}(\Omega)$  was provided in (4). Furthermore, the pairs of in-parallel bandstop sections in the connecting points between contiguous stages could be combined into a single one. This equivalent bandstop section that is shared by both stages has  $K'_B = K_B/\sqrt{2}$  as new admittance inversion coefficient between its two constituent nonresonating nodes (NRNs). Examples of theoretical power transmission and reflection responses with normalized 3-dB cutoff frequency  $\Omega_c^{3 \, dB} = 1$  for the multistage BPF scheme in Fig. 3 are depicted in Fig. 4. As can be seen, higher out-of-band rejection and lower power reflection levels are attained as the number of stages increases.

As a second procedure, the suggested symmetrical quasiabsorptive BPF principle can be applied to higher selectivity designs by using higher order bandpass and bandstop sections. This is exemplified in Fig. 5 for a *K*th-order implementation. In this case, the derivation of formulas for the coupling coefficients that allow to obtain the quasi-absorptive functionality gets more complex as the filter order increases. Hence, optimization techniques must be used for their computation

<sup>1</sup>This can be demonstrated for K = 2—and subsequently generalized to an arbitrary K value, for which

$$S_{21}^{\text{casc}}(\Omega) = \frac{[S_{21}(\Omega)]^2}{1 - [S_{11}(\Omega)]^2} \approx [S_{21}(\Omega)]^2$$
 (6)

$$\left| S_{11}^{\text{casc}}(\Omega) \right|^2 = \left| S_{11}(\Omega) + \frac{[S_{21}(\Omega)]^2 S_{11}(\Omega)}{1 - [S_{11}(\Omega)]^2} \right|^2 \ll 1 \tag{7}$$

since  $|S_{11}(\Omega)|^2 \ll 1$  and  $|S_{21}(\Omega)| \le 1$  owing to the quasi-reflectionless and passivity properties of the constituent symmetrical first-order stage.

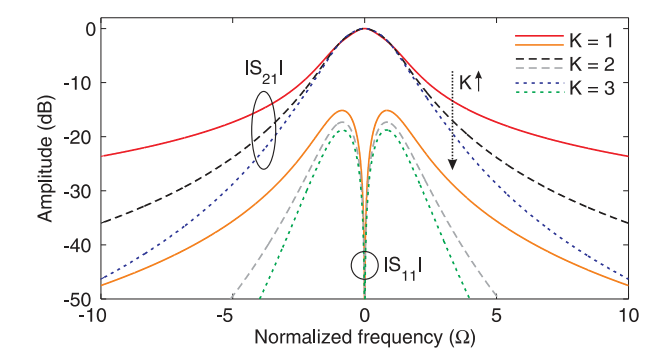


Fig. 4. Theoretical power transmission ( $|S_{21}| = |S_{12}|$ ) and reflection ( $|S_{11}| = |S_{22}|$ ) parameters of ideally synthesized examples for the multistage in-series-cascade quasi-absorptive BPF in Fig. 3 ( $K=1:K_A=1.14;K=2:K_A=1.33;$  and  $K=3:K_A=1.46$ ).

by imposing the intended 3-dB bandwidth specification for the filter and the minimization of its input power reflection throughout the entire frequency range. The theoretical power transmission and reflection parameters of illustrative secondand third-order designs of the filter scheme in Fig. 5 (i.e., K=2 and 3) are shown in Fig. 6. For comparison purposes, the power transmission and reflection responses of their second- and third-order bandpass sections and the associated two- and three-stage in-series-cascade designs (i.e., with the same normalized 3-dB cutoff frequency) are also plotted. From Fig. 6, the following conclusions are derived.

- The higher order design outperforms the multistage inseries-cascade counterpart in terms of filtering selectivity for fewer or equal number of admittance inverters (5K + 3 in Fig. 5 versus 8K in Fig. 3 that becomes 5K + 3 if the two in-parallel bandstop sections in the connecting points between contiguous stages are reduced to a single one).
- 2) The filtering selectivity of the high-order BPF arrangement in Fig. 5 is higher than that of its bandpass section. This reveals the double task of the bandstop sections in terms of not only dissipating the nontransmitted input-signal energy but also increasing the filtering selectivity when compared to that inherent to the bandpass section. In particular, for the synthesis examples in Fig. 6, close-to-passband selectivities comparable to those of Butterworth-type BPFs with the same normalized 3-dB cutoff frequency and respective fifth [example in Fig. 6(a)] and eighth [example in Fig. 6(b)] orders are obtained. Further discussion on this aspect from the digital-modeling perspective that was reported in [17] is provided in Section III-B for the second theoretically synthesized design example.

Finally, cross-coupling techniques can also be incorporated into the high-order symmetrical quasi-absorptive BPF scheme in Fig. 5 for further selectivity enhancement by means of transmission zero generation. This methodology is shown in Fig. 7 for the second-order case of the general scheme in Fig. 5, in which a source–load coupling has also been included. A comparison between the power transmission and reflection parameters of example designs for the second-order BPF network in Fig. 7 with/without nonzero cross coupling is

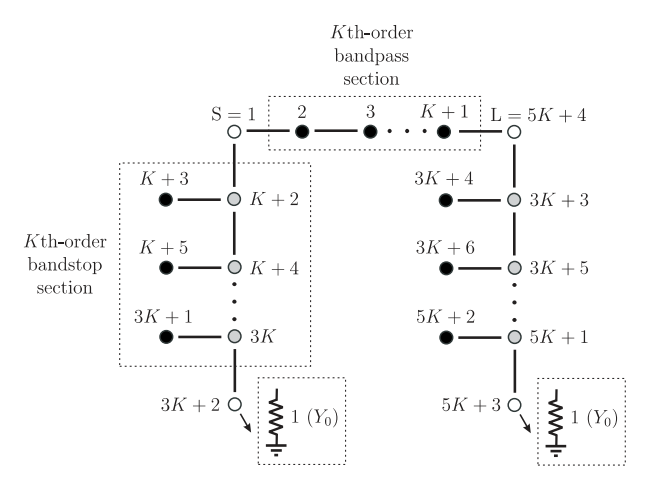


Fig. 5. Normalized coupling-routing diagram of the proposed Kth-order symmetrical quasi-reflectionless BPF [black circles: resonating nodes; gray circles: zero-susceptance NRNs; white circles: unitary source (S), load (L), and loading resistors; continuous lines: couplings; and  $Y_0 = 1/Z_0$ : reference admittance for admittance normalization].

provided in Fig. 8. As demonstrated, the filtering selectivity is considerably increased through the nonzero source—load interaction without significant influence on the power reflection profile of the filter.

#### C. Loss Influence

Since the symmetrical quasi-reflectionless BPF in Fig. 1 is shaped by a bandpass section between the input and output accesses to which the bandstop sections are connected, it is interesting to analyze the influence on the overall BPF behavior of the loss of its resonating nodes in both type of sections. For this purpose, the second-order BPF synthesis example in Fig. 6(a) has been considered for illustration purposes after including the effect of the loss in its resonating nodes. Fig. 9 represents the power transmission and reflection parameters for this design example in the cases of no loss—i.e., ideal, loss only in the bandstop sections—i.e., nonuniform-loss distribution, and loss in both the bandpass and bandstop sections—i.e., uniform-loss distribution. From Fig. 9, the following conclusions are derived.

- With the incorporation of loss in both the bandpass and bandstop sections, the expected loss effect in the overall filter is observed. It consists of the appearance of nonzero in-band insertion loss, passbandrounding effect, and reduced power reflection loss at the input/output ports.
- 2) With the inclusion of loss only in the bandstop sections, the overall BPF transfer function remains almost unaltered, whereas only a small degradation of the input/output power reflection profiles is observed.

These results reveal that mixed-technology implementations could be realized with this symmetrical quasi-reflectionless BPF approach to achieve more compact realizations without significantly sacrificing its effective quality factor (*Q*).

On the other hand, Fig. 10 provides a comparison for uniform loss distribution in all the resonating nodes between the theoretical power transmission responses of the symmetrical quasi-reflectionless BPF—second-order example

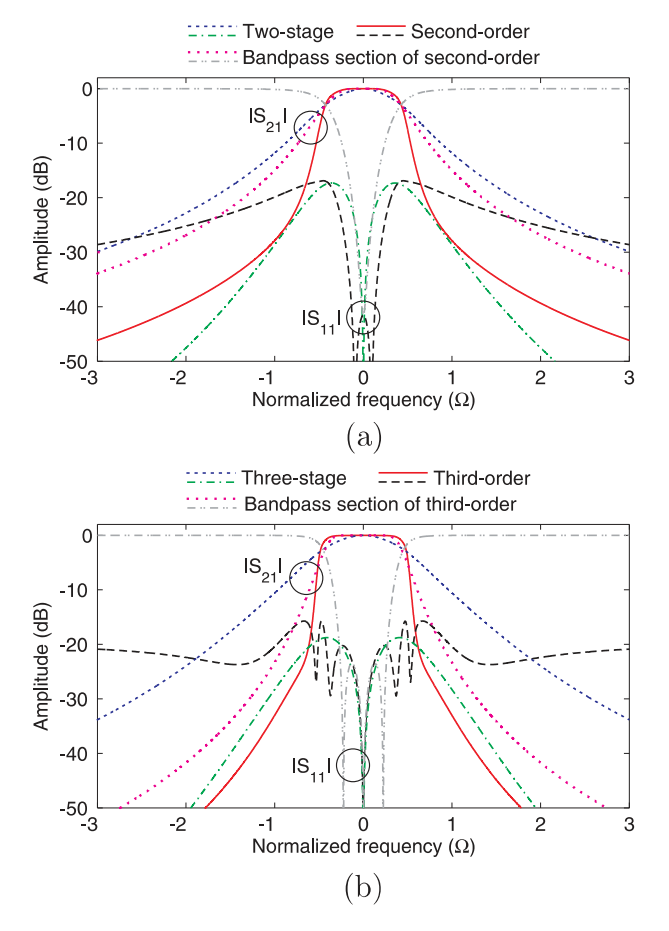


Fig. 6. Theoretical power transmission ( $|S_{21}| = |S_{12}|$ ) and reflection ( $|S_{11}| = |S_{22}|$ ) parameters of the ideally synthesized second- and third-order examples of the *K*th-order symmetrical quasi-reflectionless BPF in Fig. 5, their bandpass sections, and their associated two- and three-stage in-series-cascade BPF designs as in Fig. 3. (a) Second-order BPF:  $M_{1,2} = M_{3,14} = 0.55$ ,  $M_{1,4} = M_{9,14} = 1$ ,  $M_{2,3} = 0.3$ ,  $M_{4,5} = M_{9,10} = 0.8$ ,  $M_{4,6} = M_{9,11} = 1$ ,  $M_{6,7} = M_{11,12} = 0.75$ , and  $M_{6,8} = M_{11,13} = 1$ . Two-stage BPF:  $K_A = 0.867$ . (b) Third-order BPF:  $M_{1,2} = M_{4,19} = 0.6$ ,  $M_{1,5} = M_{12,19} = 0.94$ ,  $M_{2,3} = M_{3,4} = 0.3$ ,  $M_{5,6} = M_{12,13} = 0.8$ ,  $M_{5,7} = M_{12,14} = 0.94$ ,  $M_{7,8} = M_{14,15} = 0.95$ ,  $M_{7,9} = M_{14,16} = 1$ ,  $M_{9,10} = M_{16,17} = 0.75$ , and  $M_{9,11} = M_{16,18} = 0.9$ . Three-stage BPF:  $K_A = 1.021$ .

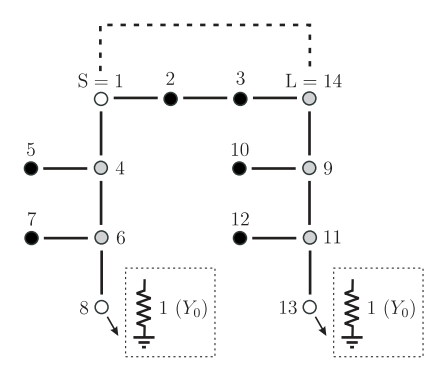


Fig. 7. Second-order case of the *K*th-order symmetrical quasi-reflectionless BPF in Fig. 5 with the inclusion of source–load coupling (dashed line).

in Fig. 6(a)—and a classic fifth-order Butterworth-type BPF with reflective nature that exhibits the same normalized bandwidth and comparable close-to-passband cutoff-slope sharpness. As can be seen, the quasi-reflectionless behavior is realized in the engineered BPF architecture at the expense of

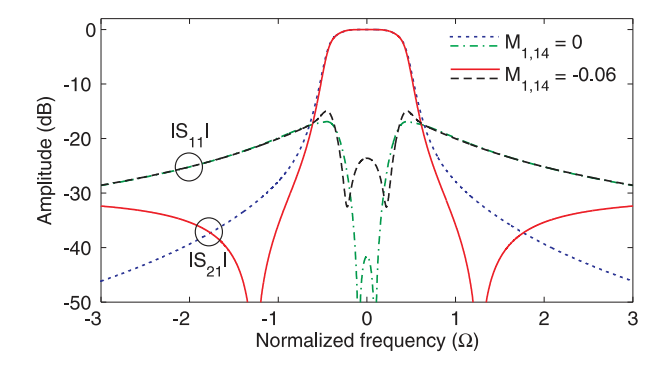


Fig. 8. Theoretical power transmission ( $|S_{21}| = |S_{12}|$ ) and reflection ( $|S_{11}| = |S_{22}|$ ) parameters of ideally synthesized examples for the second-order symmetrical quasi-reflectionless BPF in Fig. 7 with/without nonzero source–load coupling ( $M_{1,2} = M_{3,14} = 0.55$ ,  $M_{1,4} = M_{9,14} = 1$ ,  $M_{2,3} = 0.3$ ,  $M_{4,5} = M_{9,10} = 0.8$ ,  $M_{4,6} = M_{9,11} = 1$ ,  $M_{6,7} = M_{11,12} = 0.75$ , and  $M_{6,8} = M_{11,13} = 1$  for both designs).

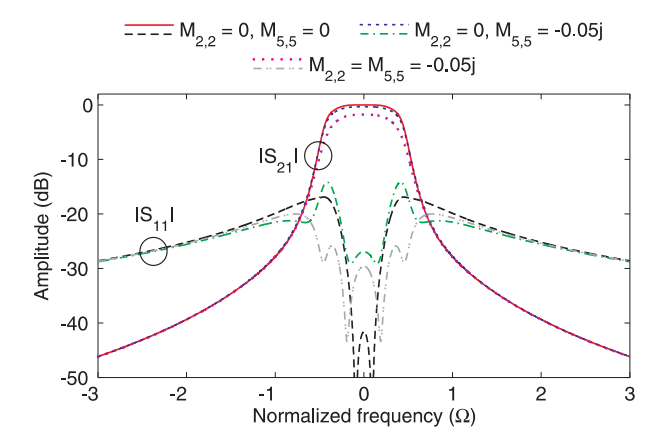


Fig. 9. Effect of the loss of the resonating nodes in the theoretical power transmission ( $|S_{21}| = |S_{12}|$ ) and reflection ( $|S_{11}| = |S_{22}|$ ) parameters of ideally synthesized example in Fig. 6(a) ( $M_{2,2} = M_{3,3}$  and  $M_{5,5} = M_{7,7} = M_{10,10} = M_{12,12}$  for all responses). Note that  $M_{k,k} = -0.05j = 1/(j\Delta Q_k)$  corresponds, e.g., to a quality factor  $Q_k = 200$  of the kth resonating node for a relative bandwidth  $\Delta = 0.1$  in the ideal BPF [18], [19].

lower out-of-band rejection levels, reduced in-band amplitude flatness, especially at the passband edges due to the influence of the quasi-absorptive bandstop sections, and slightly increased minimum in-band power insertion loss (0.35 dB versus 0.28 dB for  $M_{k,k} = -0.01j$  and 3.51 dB versus 2.81 dB for  $M_{k,k} = -0.1j$ , which respectively correspond, e.g., to a quality factor  $Q_k = 1/(j\Delta M_{k,k})$  of 1000 and 100 in all the resonating nodes for a relative bandwidth  $\Delta = 0.1$ ).

## D. Comparison With Prior Art Reflectionless Bandpass Filters

The proposed symmetrical quasi-reflectionless BPF architecture is compared here with some prior art reflectionless BPF structures, such as the input-fully reflectionless BPF in [15] and the symmetrical fully reflectionless BPF in [12] and [13].

Fig. 11 shows the power transmission and reflection responses of the first-order symmetrical quasi-absorptive BPF section in Fig. 1 and the input-reflectionless BPF section in [15, Fig. 1] for synthesized examples with 3-dB normalized cutoff frequency equal to one. As can be seen, whereas the example corresponding to the approach in [15] features

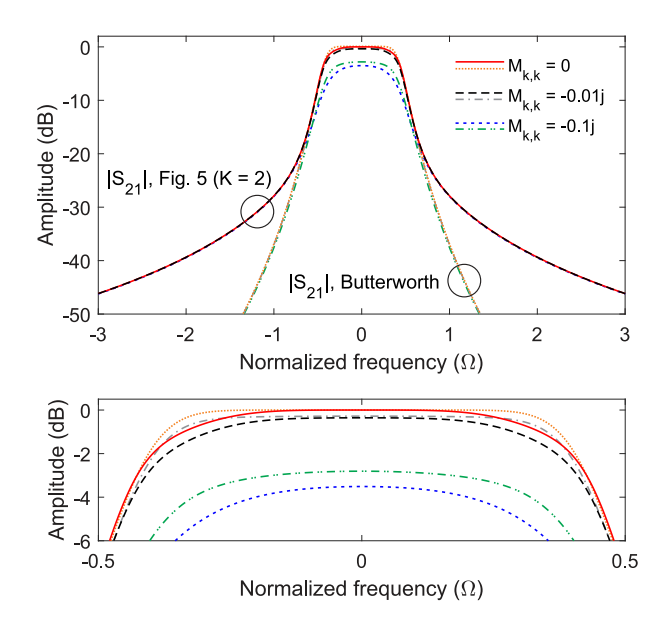


Fig. 10. Comparison between the theoretical power transmission ( $|S_{21}| = |S_{12}|$ ) responses of the second-order example in Fig. 6(a) and a classic fifth-order Butterworth-type BPF that exhibits the same fractional bandwidth and close-to-passband cutoff-slope sharpness for  $M_{k,k} = 0$ , -0.01j, and -0.1j in all the resonating nodes (broadband and passband detail representation).

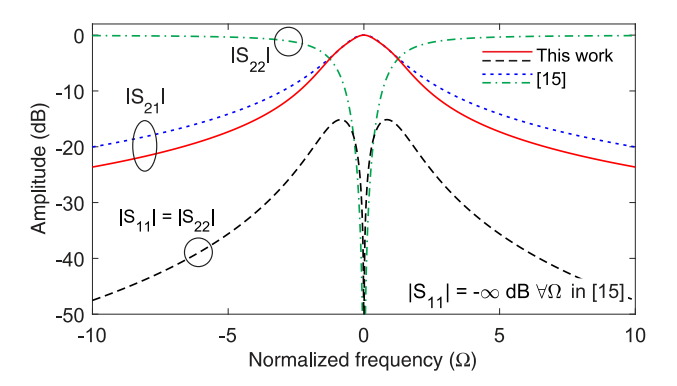


Fig. 11. Power transmission ( $|S_{21}|$ ) and reflection ( $|S_{11}|$  and  $|S_{22}|$ ) responses of theoretical synthesized examples for the first-order symmetrical quasi-absorptive BPF section in Fig. 1 of this paper ( $K_A = 1.14$ ) and the first-order input fully reflectionless BPF section in Fig. 1 of [15] ( $K_A = 1$ ).

zero power reflection at all frequencies at the input port but a reflective-type nature at the output port, the symmetrical quasi-absorptive example of this paper exhibits quasi-reflectionless behavior at both ports. Furthermore, higher out-of-band power attenuation levels are obtained for the example of the current work owing to the action of the additional resonating node—three resonating nodes in total—with regard to the one in [15]—two resonating nodes in total—for the first-order BPF section.

Subsequently, the engineered symmetrical quasi-absorptive BPF concept is compared with the symmetrical fully reflectionless BPF topology in [13]. Note that the first-order fully reflectionless BPF section in [13], which can be obtained after a lowpass-to-bandpass frequency transformation of the lowpass circuit in Fig. 1(d) therein, differs from the current one as follows: 1) it comprises six resonators—three series-type and three parallel-type resonators—and 2) it exhibits a two-path transversal configuration. Hence, for a fair comparison,

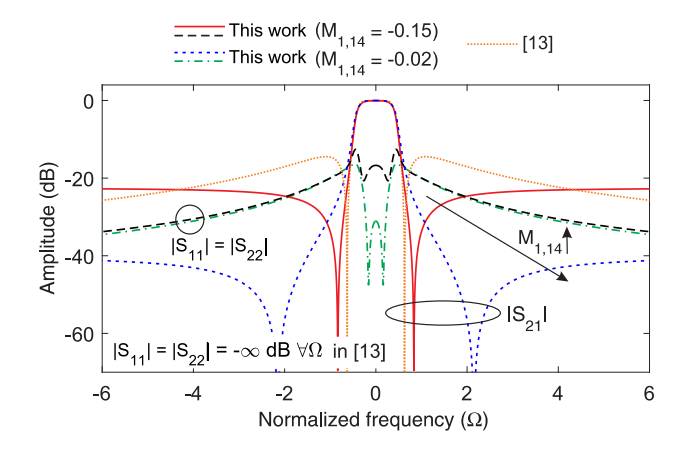


Fig. 12. Power transmission ( $|S_{21}|$ ) and reflection ( $|S_{11}|$  and  $|S_{22}|$ ) responses of theoretical synthesized examples for the second-order symmetrical quasi-absorptive BPF scheme in Fig. 7 of this paper (all the parameter values are as in the example in Fig. 8 except for  $M_{1,14}$ ) and the first-order fully reflectionless BPF section in Fig. 1(d) of [13] (normalized transmission zero frequency  $\Omega_z = 0.628$ ).

the second-order symmetrical quasi-reflectionless example in Fig. 7 with nonzero source—load coupling for the generation of the additional signal-propagation path is considered. Fig. 12 depicts the power transmission and reflection responses of theoretical examples with the same 3-dB normalized cutoff frequency for both cases. From this paper and the analysis of the two approaches, the following conclusions can be obtained.

- 1) The variation of the magnitude of the source-load coupling allows to flexibly allocate the symmetrical transmission zeros while keeping a nearly similar bandwidth, leading to designable higher attenuation levels in some spectral regions depending on the specification. This is not feasible in the first-order symmetrical fully reflectionless BPF section in [13, Fig. 1(d)], where the stopband transmission zero position directly determines the synthesized bandwidth. This design weakness was also proven in [20], which reveals that there is no control over the edge of the stopband once the transmission zero location is fixed.
- 2) The proposed symmetrical quasi-reflectionless BPF principle is formulated through a coupling-matrix formalism with parallel-type resonators and admittance inverters, which allows its direct extrapolation to any technology. Moreover, as shown in Section III-A, structures with/without cross coupling can be considered to realize different types of filtering profiles including linear-phase ones. However, in the approach in [13], only some specific networks—e.g., transmission-line-based first-order section or lumped-element-based second/third-order cells and associated in-series cascades—are presented.
- 3) For moderate-to-narrow-bandwidth BPF designs, the transmission-line-based first-order BPF section in [13, Fig. 3(f)] may be unrealizable in practice due to the large ratio needed between the  $Z_1$  and  $Z_2$  characteristic-impedance parameters of the stubs— $Z_1/Z_2 = 4\rho(\rho+1)^2/(\rho-1)^4$  where  $\rho$  is the coupling coefficient of the coupled-line section. For example, for a 10% 3-dB fractional bandwidth,  $\rho=1.96$  that

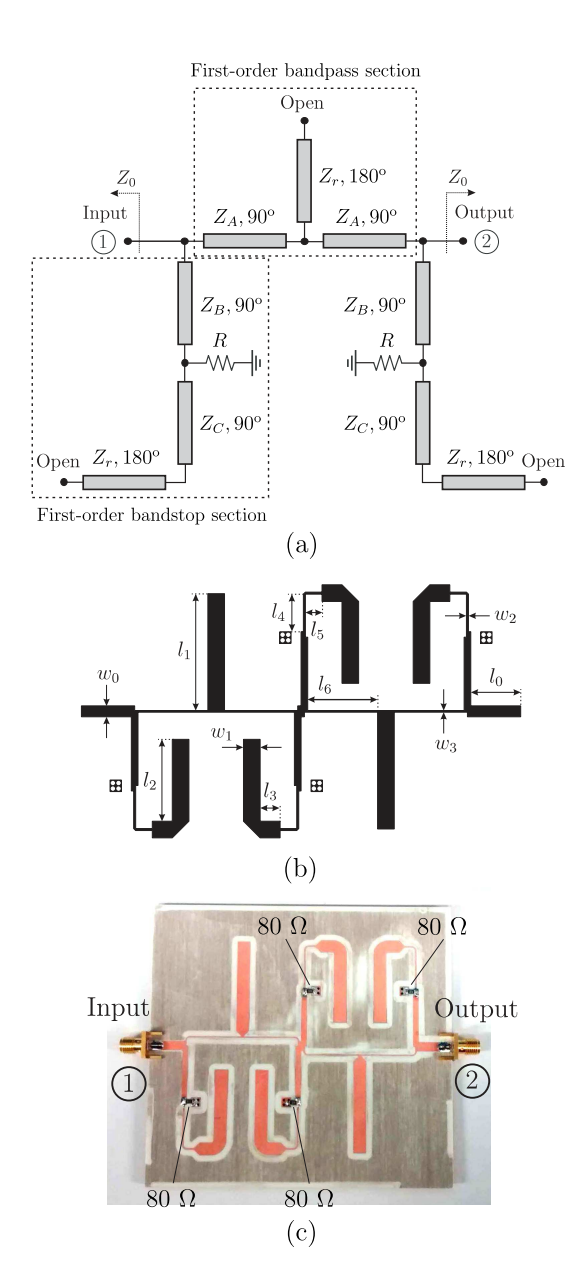


Fig. 13. Manufactured two-stage in-series-cascade quasi-absorptive microstrip BPF prototype (RO4350B substrate). (a) Ideal transmission-line circuit schematic of its constituent first-order stage ( $Z_A=125~\Omega,~Z_B=70~\Omega,~Z_C=115~\Omega,~R=80~\Omega,~Z_0=50~\Omega,~$  and electrical lengths given at 2.5 GHz). (b) Layout (nonredundant dimensions in millimeter:  $w_0=3.3,~w_1=1.92,~w_2=0.42,~w_3=0.56,~w_4=4.5,~l_0=15,~l_1=17.6,~l_2=20.9,~l_3=18.6,~l_4=32.8,~l_5=33.6,~$  and taper length: 4 mm). (c) Photograph.

results in  $Z_1 = 8.9931Z_0$  and  $Z_2 = 0.1112Z_0$ —i.e.,  $Z_1/Z_2 = 80.87$ . Such limitation can also be observed in [21, Fig. 4], which also addresses distributed-element implementations of such first-order fully absorptive BPF.

#### III. EXPERIMENTAL RESULTS

For experimental-demonstration purposes of the described quasi-absorptive RF BPF design principle, two different 50- $\Omega$ -referred BPF prototypes have been manufactured in microstrip technology and characterized. For the practical development of the first circuit—Prototype 1, an RO4350B microstrip substrate with the following characteristics was used: relative dielectric permittivity  $\varepsilon_r = 3.48$ , dielectric thickness

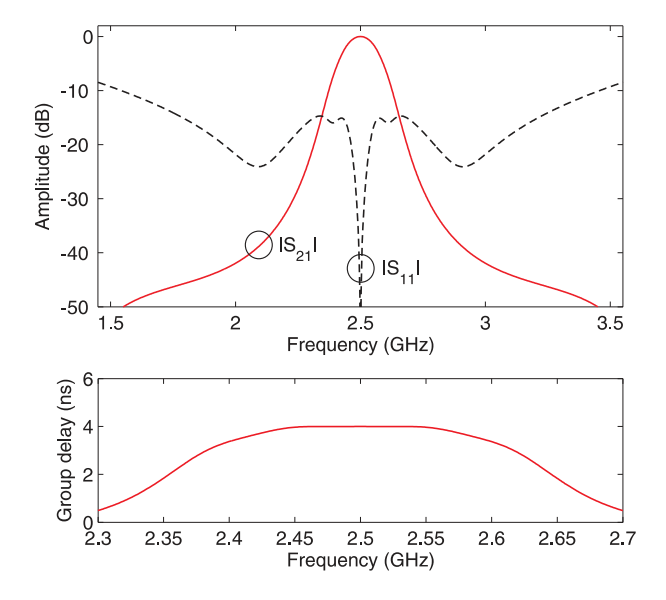


Fig. 14. Ideal power transmission ( $|S_{21}|$ ), reflection ( $|S_{11}|$ ), and group-delay responses of the theoretically synthesized two-stage in-series-cascade quasi-absorptive BPF example.

H=1.52 mm, metal thickness  $t=17.8~\mu$ m, and dielectric loss tangent  $\tan \delta_D = 0.0031$ ; for the second circuit—Prototype 2, an RO4003C microstrip substrate was employed whose main parameters are  $\varepsilon_r = 3.38$ , H=1.52 mm,  $t=17.8~\mu$ m, and  $\tan \delta_D = 0.0027$ . The ground connections were implemented as 1-mm-diameter metallic via holes, whereas resistors from Panasonic were employed.

The ideal design process for both BPF prototypes started from the derivation of their normalized coupling-routing diagrams, followed by a normalized-lowpass-to-bandpass frequency transformation as well as the admittance scaling of their input-/output-port admittances, resonating nodes, and NRNs. The resonators and admittance inverters were physically realized through conventional RF filter implementation techniques [18], [19]. The two fabricated BPF prototypes were optimized and simulated with the software package Keysight ADS. Their measurements in terms of *S*-parameters were made by means of an Agilent E8361A network analyzer and include the effects of the input/output SMA connectors.

## A. Prototype 1

The first microstrip prototype corresponds to a two-stage in-series-cascade BPF with flat in-band group delay. It should be remarked upon that, up to now, only a very few inband-linear-phase quasi-reflectionless BPF architectures have been proposed as the one described in [22], which was experimentally verified in the lower region of the microwave band in a multilayer implementation. The designed filter was ideally synthesized to be centered at 2.5 GHz and to exhibit a 3-dB absolute bandwidth equal to 145 MHz (i.e., equal to 5.8% in relative terms). Its admittance inverters were realized as quarter-wavelength at 2.5-GHz transmission-line segments whose characteristic impedances are as follows:  $Z_A = 125 \Omega$ ,  $Z_B = 70 \Omega$ , and  $Z_C = 115 \Omega$  ( $Z_0 = 50 \Omega$ )—see Fig. 13(a). They were computed as  $Z = Z_0/M$ , where M is the coupling coefficient associated with each admittance inverter.

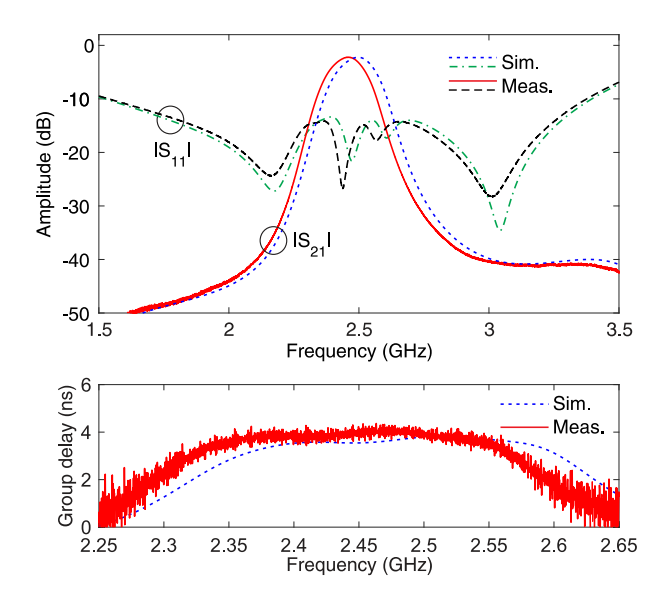


Fig. 15. Simulated and measured power transmission ( $|S_{21}|$ ), reflection ( $|S_{11}|$ ), and group-delay responses of the manufactured two-stage in-series-cascade quasi-absorptive microstrip BPF prototype.

The resonating nodes were implemented as open-ended halfwavelength at 2.5-GHz transmission-line segments with characteristic impedance  $Z_r = 40 \Omega$  to meet the passband-width specification. Note that, in this particular design, the admittance inverters between the NRN, resonating node, and loading resistor in each first-order bandstop section were optimized to achieve the intended in-band linear-phase behavior. In particular, 80- $\Omega$  loading resistors were directly attached to the NRNs of the first-order bandstop sections to save four admittance inverters in the overall quasi-absorptive BPF circuit. The power transmission, reflection, and in-band group-delay profiles of this theoretically synthesized two-stage in-seriescascade quasi-absorptive BPF example are depicted in Fig. 14. Note that the obtaining of zero power reflection in all the frequency range is not feasible due to several aspects, such as the frequency dependence of the real admittance inverters not considered by the coupling-matrix formalism, deviations in the values of the commercial components from the ideal ones, and fabrication tolerances. In this case, input-power-matching levels above 15.1 and 10 dB are, respectively, attained within the 3-dB BPF bandwidth and the 1.54-3.46-GHz frequency interval—i.e., 2.25:1 ratio.

The ideal transmission-line circuit schematic for the constituent first-order stage, layout, and a photograph of the developed prototype are shown in Fig.13. Its simulated and measured *S*-parameters and in-band group-delay curve are represented in Fig. 15. As observed, apart from a minor shifting down of the measured response due to the substrate tolerance, a reasonably close agreement between simulations and measurements is obtained. The main measured performances of this BPF circuit are as follows: center frequency of 2.45 GHz, 3-dB absolute bandwidth equal to 148.3 MHz (i.e., of 6% in relative terms), minimum in-band power insertion-loss level of 2.2 dB, minimum input-power-matching levels of 14.8 and 10 dB within the 3-dB bandwidth and 1.54–3.38-GHz spectral

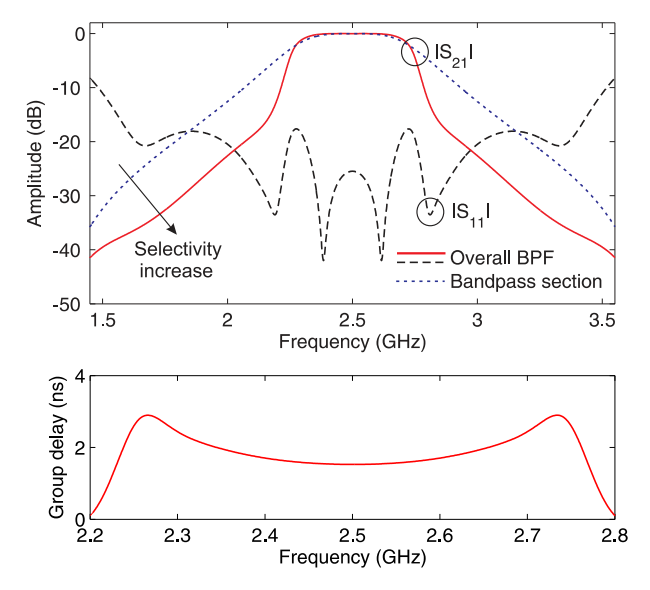


Fig. 16. Ideal power transmission ( $|S_{21}|$ ), reflection ( $|S_{11}|$ ), and group-delay responses of the theoretically synthesized second-order quasi-absorptive BPF example and transfer function of its constituent second-order bandpass section.

range—i.e., 2.2:1 ratio, respectively, and minimum group-delay variation of 0.4 ns—in-band group-delay in the range of  $4 \pm 0.2$  ns—within the measured 3-dB filter bandwidth.

## B. Prototype 2

The second microstrip prototype is a 2.5-GHz secondorder quasi-absorptive BPF with a 3-dB absolute bandwidth equal to 475 MHz (i.e., of 19% in relative terms). The ideal design parameter values of this BPF circuit, which were mainly obtained through optimization as in the high-order filter synthesis examples in Fig. 6 in Section II-B, are as follows:  $Z_{1,2} = 80 \Omega$ ,  $Z_{2,3} = 135 \Omega$ ,  $Z_{1,4} = 55 \ \Omega$ ,  $Z_{4,5} = Z_{4,6} = Z_{6,8} = 50 \ \Omega$ , and  $Z_{6,7} = 60 \ \Omega$  $(Z_0 = 50 \ \Omega)$ —see Fig. 18(a). Its admittance inverters and resonating nodes were physically realized as in the first prototype, whereas the  $50-\Omega$  resistor that loads each second-order bandstop section was directly connected to its nearest NRN since its adjacent inverter (impedance  $Z_{6,8} = Z_0$ ) can be omitted. The power transmission, reflection, and in-band group-delay responses of this theoretically synthesized second-order quasiabsorptive BPF example are plotted in Fig. 16. As can be seen, input-power-matching levels higher than 17.6 and 10 dB are, respectively, obtained within the 3-dB BPF bandwidth and the 1.48–3.52-GHz frequency interval—i.e., 2.38:1 ratio.

For comparison purposes, the theoretical transfer function of the isolated bandpass section is also represented in Fig. 16. The selectivity increase produced by the absorptive bandstoptype branches in the overall BPF, as it was anticipated in Section II-B, can be appreciated. From the application of the behavioral-digital-modeling technique in [17], it is possible to quantify this selectivity-enhancement effect by comparing the number of poles in the transfer functions of linear-time-invariant digital systems associated with the overall BPF and the isolated bandpass section whose formulation is as follows:

$$H(z) = \frac{\sum_{k=0}^{M} b_k z^{-k}}{\sum_{k=0}^{N} a_k z^{-k}}$$
 (8)

TABLE I COEFFICIENTS  $a_k$  and  $b_k$  of the Digital System Associated With the Second-Order Quasi-Absorptive BPF Example

Coefficient Values							
k	$a_k$	$b_k$	k	$a_k$	$b_k$		
0	+1.0000	+0.0715	12	+0.8048	+0.0120		
1	-1.5282	-0.0835	13	-0.7434	+0.0204		
2	-0.2839	+0.1052	14	+0.0853	+0.0207		
3	+3.8445	-0.0020	15	+0.3947	+0.0177		
4	-2.8900	-0.0106	16	-0.1985	+0.0164		
5	-2.1825	+0.1111	17	-0.0137	-0.0087		
6	+4.9844	+0.0047	18	+0.0341	+0.0109		
7	-1.5650	-0.0226	19	-0.0122	+0.0028		
8	-2.2457	+0.1117	20	+0.0340	+0.0062		
9	+2.4200	-0.0212	21	+0.0029	-		
10	-0.6704	+0.0656	22	-0.0144	_		
11	-0.3525	+0.0220	23	-0.0038	_		

TABLE II

Coefficients  $a_k$  and  $b_k$  of the Digital System Associated With the Isolated Second-Order Bandpass Section of the Second-Order Quasi-Absorptive BPF Example

Coefficient Values								
k	$a_k$	$b_k$	k	$a_k$	$b_k$			
0	+1.0000	+0.1739	4	-0.3513	+0.1739			
1	-0.6536	+0.0000	5	-0.2195	_			
2	-0.1813	+0.3477	6	+0.2285	_			
3	+0.9259	+0.0000	7	-0.0533	_			

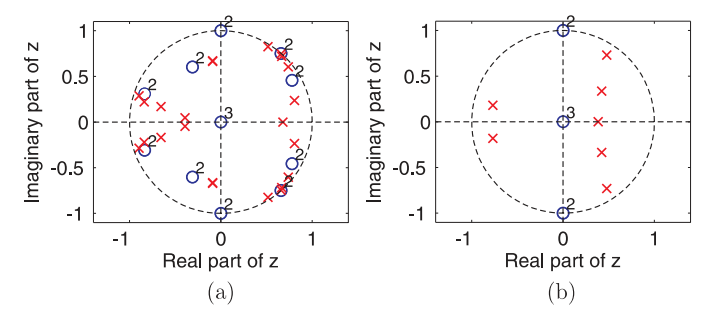


Fig. 17. Zero-pole diagrams in the z plane of the digital LTI systems associated with the transfer functions in Fig. 16 (o: zero;  $\times$ : pole; number: zero/pole multiplicity). (a) Overall BPF. (b) Bandpass section.

where  $z=e^{j\Omega}$  is a complex variable,  $\Omega=\pi f/f_d$  is the normalized frequency, and M and N are the order of the numerator and denominator polynomials in the variable z. The coefficients  $a_k$  and  $b_k$  extracted for both transfer functions are listed in Tables I and II, whereas their zero-pole diagrams are represented in Fig. 17. As observed, 16 poles more are obtained in the overall BPF—23 poles in total—with regard to its isolated second-order bandpass section—7 poles in total.

The ideal transmission-line circuit schematic, layout, and a photograph of the constructed prototype are given in Fig. 18. Its simulated and measured *S*-parameters and in-band group-delay profile are depicted in Fig. 19. As can be seen, apart from some discrepancies observed in the input power-matching levels for the upper stopband due to manufacturing tolerances, the agreement obtained between simulations and

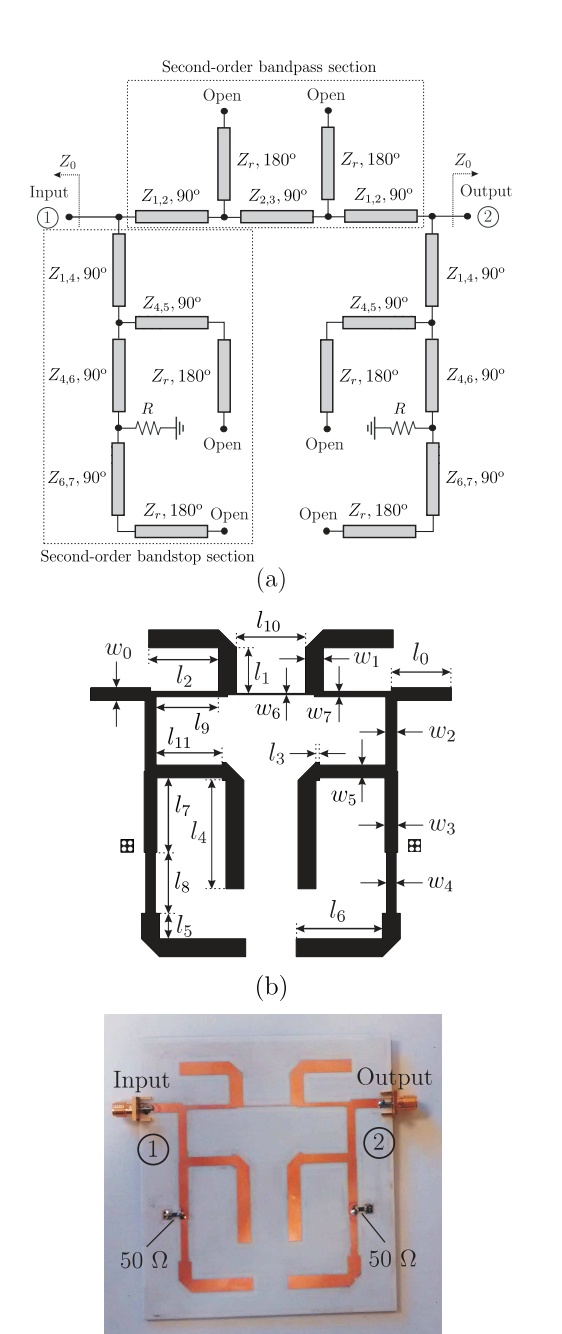


Fig. 18. Manufactured second-order quasi-absorptive microstrip BPF prototype (RO4003C substrate). (a) Ideal transmission-line circuit schematic ( $Z_{1,2}=80~\Omega,~Z_{2,3}=135~\Omega,~Z_{1,4}=55~\Omega,~Z_{4,5}=Z_{4,6}=Z_{6,8}=50~\Omega$ — $Z_{6,8}$  is absorbed into the resistor,  $Z_{6,7}=60~\Omega,~R=50~\Omega,~Z_{0}=50~\Omega,~$  and electrical lengths given at 2.5 GHz). (b) Layout (nonredundant dimensions in millimeter:  $w_0=3.3,~w_1=4.9,~w_2=3,~w_3=3.48,~w_4=2.6,~w_5=3.48,~w_6=0.34,~w_7=1.46~l_0=15,~l_1=12,~l_2=19.2,~l_3=1,~l_4=29.8,~l_5=7,~l_6=23.7,~l_7=20.5,~l_8=16.8,~l_9=17.2,~l_{10}=19,~$  and  $l_{11}=18$ ). (c) Photograph.

(c)

measurements is reasonably close. Thus, the proposed concept is again verified.

The main measured performances of this prototype are as follows: center frequency equal to 2.49 GHz, 3-dB absolute bandwidth of 455 MHz (i.e., of 18.2% in relative terms), minimum in-band power insertion-loss level of 0.9 dB, minimum input-power-matching levels of 11.5 and 10 dB within

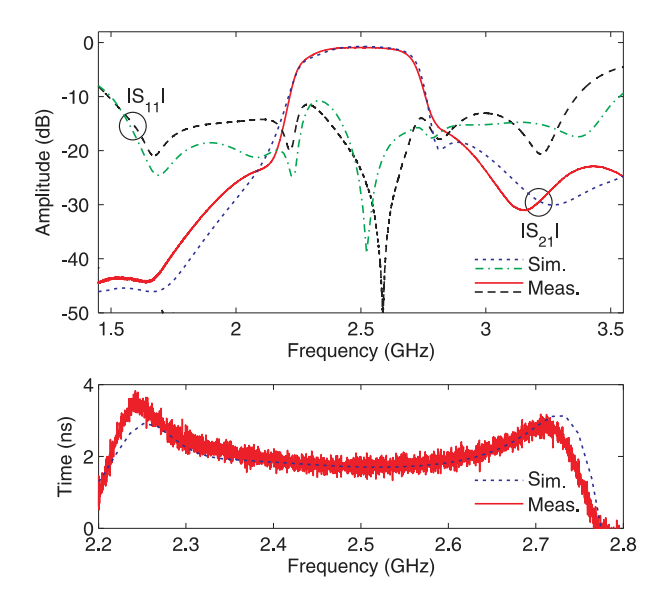


Fig. 19. Simulated and measured power transmission ( $|S_{21}|$ ), reflection ( $|S_{11}|$ ), and group-delay responses of the manufactured second-order quasi-absorptive microstrip BPF prototype.

the 3-dB bandwidth and 1.49–3.36-GHz spectral range—i.e., 2.26:1 ratio, respectively, and in-band group-delay variation within the measured 3-dB bandwidth of the filter below 1.5 ns.

#### IV. CONCLUSION

A class of symmetrical quasi-absorptive RF BPFs has been reported. They can eliminate the need for nonreciprocal devices, such as interstage isolation circuits to protect RF active circuits from undesired reflected signals, in complete RF transceivers. The engineered filter approach is shaped by the main bandpass section and nearly complementary bandstop sections at its input/output ports that are loaded with resistors. In this manner, most of the nontransmitted inputsignal energy is nearly dissipated by the loading resistors of the bandstop sections to achieve the quasi-absorptive functionality. Moreover, the input/output bandstop sections allow to increase the overall filtering selectivity with regard to the one provided by the bandpass section itself. The theoretical foundations of the first-order symmetrical quasi-absorptive BPF stage have been described. In addition, ideal synthesis examples of higher rejection designs based on the in-series cascade of several first-order stages, as well as higher selectivity schemes with higher order filtering sections and cross coupling, have been presented. For experimental-validation purposes, two 2.5-GHz symmetrical quasi-absorptive microstrip BPF prototypes have been developed and characterized. They consist of the direct in-series cascade of two identical first-order stages with overall in-band flat-group-delay behavior and a second-order design.

#### APPENDIX

This appendix demonstrates that the symmetrical BPF architecture in Fig. 1 cannot exhibit a fully reflectionless behavior in the entire normalized frequency range  $\Omega \in [-\infty, +\infty]$ .

From (5), it comes to light that the attaining of a perfectly reflectionless (i.e.,  $S_{11}(\Omega) = S_{22}(\Omega) = 0$ ,  $\forall \Omega$ ) bandpass-filtering operation for the symmetrical BPF network in Fig. 1

implies the following constraint for the normalized-to- $Y_0$  evenand odd-mode admittances  $Y_e(\Omega)$  and  $Y_o(\Omega)$  to be satisfied:

$$Y_e(\Omega) Y_o(\Omega) = 1 \quad \forall \Omega.$$
 (A.1)

From (1) and (2), it can be easily deduced that the fulfillment of (A.1) results into the three following conditions to be met

$$M_{1,3}^4 = M_{3,5}^4 \tag{A.2}$$

$$M_{1,2}^2 M_{1,3}^2 M_{3,5}^2 = M_{3,4}^2 M_{3,5}^2 \tag{A.3}$$

$$M_{1,3}^4 = M_{3,5}^4 \qquad (A.2)$$

$$M_{1,2}^2 M_{1,3}^2 M_{3,5}^2 = M_{3,4}^2 M_{3,5}^2 \qquad (A.3)$$

$$2M_{1,2}^2 M_{1,3}^2 M_{3,4}^2 = M_{3,4}^4. \qquad (A.4)$$

By noting that  $M_{3,5} \neq 0$  (i.e., the dissipative resistors must be connected to the BPF), it is derived from (A.2) that  $M_{1,3} \neq 0$ . On the other hand, from (A.3) and (A.4) and taking into account that  $M_{1,3} \neq 0$ , it turns out that  $M_{3,4} = 0$ ineludibly leads to  $M_{1,2} = 0$ . However, the fact that  $M_{1,2} = 0$ so that the conditions (A.2)-(A.4) are satisfied results in the absurdity that there is no signal-transmission path between the source and the load in the BPF structure in Fig. 1. Hence, for reductio ad absurdum, the symmetrical BPF scheme in Fig. 1 cannot be fully absorptive at all normalized frequencies  $\Omega$ .

## REFERENCES

- [1] R. Gómez-García, F. M. Ghannouchi, N. B. Carvalho, and H. C. Luong, "Guest editorial: Advanced circuits and systems for CR/SDR applications," IEEE J. Emerg. Sel. Topics Circuits Syst., vol. 3, no. 4, pp. 485-488, Dec. 2013.
- [2] W. J. Chappell, E. J. Naglich, C. Maxey, and A. C. Guyette, "Putting the radio in 'software-defined radio': Hardware developments for adaptable RF systems," Proc. IEEE, vol. 102, no. 3, pp. 307-320, Mar. 2014.
- [3] D. Psychogiou, R. Gómez-García, and D. Peroulis, "Fully-reconfigurable bandpass/bandstop filters and their coupling-matrix representation," IEEE Microw. Wireless Compon. Lett., vol. 26, no. 1, pp. 22-24, Jan. 2016.
- [4] R. Gómez-García and A. C. Guyette, "Reconfigurable multi-band microwave filters," IEEE Trans. Microw. Theory Techn., vol. 63, no. 4, pp. 1294-1307, Apr. 2015.
- [5] R. Gómez-García, R. Loeches-Sánchez, D. Psychogiou, and D. Peroulis, "Multi-stub-loaded differential-mode planar multiband bandpass filters," IEEE Trans. Circuits Syst. II, Exp. Briefs, vol. 65, no. 3, pp. 271–275, Mar. 2018.
- [6] D. Psychogiou, R. Gómez-García, and D. Peroulis, "RF wide-band bandpass filter with dynamic in-band multi-interference suppression capability," IEEE Trans. Circuits Syst. II, Exp. Briefs, vol. 65, no. 5, pp. 898–902, Jul. 2018.
- [7] B. Mini-Circuits, "Reflectionless filters improve linearity and dynamic range," Microw. J., vol. 58, no. 8, pp. 42-50, Aug. 2015.
- [8] N. A. Estep, D. L. Sounas, and A. Alù, "Magnetless microwave circulators based on spatiotemporally modulated rings of coupled resonators," IEEE Trans. Microw. Theory Techn., vol. 64, no. 2, pp. 502-518, Feb. 2016.
- [9] D. R. Jachowski, "Compact, frequency-agile, absorptive bandstop filters," in IEEE MTT-S Int. Microw. Symp. Dig. Long Beach, CA, USA, Jun. 2005, pp. 513-516.
- [10] D. Psychogiou, R. Gómez-García, and D. Peroulis, "Acoustic-wavelumped-element-resonator filters with equi-ripple absorptive stopbands," IEEE Microw. Wireless Compon. Lett., vol. 26, no. 3, pp. 177-179, Mar. 2016.
- [11] A. C. Guyette, I. C. Hunter, and R. D. Pollard, "Design of absorptive microwave filters using allpass networks in a parallel-cascade configuration," in IEEE MTT-S Int. Microw. Symp. Dig., Boston, MA, USA, Jun. 2009, pp. 733-736.
- [12] M. A. Morgan and T. A. Boyd, "Theoretical and experimental study of a new class of reflectionless filter," IEEE Trans. Microw. Theory Techn., vol. 59, no. 5, pp. 1214-1221, May 2011.
- [13] M. A. Morgan and T. A. Boyd, "Reflectionless filter structures," IEEE Trans. Microw. Theory Techn., vol. 63, no. 4, pp. 1263-1271, Apr. 2015.

- [14] T.-H. Lee, B. Lee, and J. Lee, "First-order reflectionless lumped-element lowpass filter (LPF) and bandpass filter (BPF) design," in Proc. IEEE MTT-S Int. Microw. Symp. (IMS), San Francisco, CA, USA, May 2016, pp. 1-4.
- [15] D. Psychogiou and R. Gómez-García, "Reflectionless adaptive RF filters: Bandpass, bandstop, and cascade designs," IEEE Trans. Microw. Theory Techn., vol. 65, no. 11, pp. 4593-4605, Nov. 2017.
- A. Atia, A. Williams, and R. Newcomb, "Narrow-band multiple-coupled cavity synthesis," IEEE Trans. Circuits Syst., vol. 21, no. 5, pp. 649-655, Sep. 1974.
- [17] J.-M. Muñoz-Ferreras and R. Gómez-García, "A digital interpretation of frequency-periodic signal-interference microwave passive filters,' IEEE Trans. Microw. Theory Techn., vol. 62, no. 11, pp. 2633-2640, Nov. 2014.
- [18] I. C. Hunter, Theory and Design of Microwave Filters. London, U.K.: IEE Press, 2001.
- [19] J.-S. Hong, Microstrip Filters for RF/Microwave Applications, 2nd ed. New York, NY, USA: Wiley, 2011.
- [20] S. C. D. Roy, "Comments on 'theoretical and experimental study of a new class of reflectionless filter," IEEE Trans. Microw. Theory Techn., vol. 60, no. 3, pp. 632-633, Mar. 2012.
- C. Jackson, "Transmission line replacements for a lumped element reflectionless filter," in Proc. IEEE Radio Wireless Symp. (RWS), Newport Beach, CA, USA, Jan. 2014, pp. 166-168.
- [22] A. R. Djordjevic and A. G. Zajic, "Low-reflection bandpass filters with a flat group delay," IEEE Trans. Microw. Theory Techn., vol. 53, no. 4, pp. 1164-1167, Apr. 2005.



Roberto Gómez-García (S'02-M'06-SM'11) was born in Madrid, Spain, in 1977. He received the degree in telecommunication engineering and the Ph.D. degree in electrical and electronic engineering from the Polytechnic University of Madrid, Madrid, in 2001 and 2006, respectively.

He was with the C2S2 Department, XLIM Research Institute, University of Limoges, Limoges, France; the Telecommunications Institute, University of Aveiro, Aveiro, Portugal; the U.S. Naval Research Laboratory, Microwave Technology Branch, Wash-

ington, DC, USA; and Purdue University, West Lafayette, IN, USA. Since 2006, he has been an Associate Professor with the Department of Signal Theory and Communications, University of Alcalá, Alcalá de Henares, Spain. He is currently an Adjunct Part-Time Professor with the University of Electronic Science and Technology of China, Chengdu, China. His current research interests include the design of fixed/tunable high-frequency filters and multiplexers in planar, hybrid, and monolithic microwave-integrated circuit technologies, multifunction circuits and systems, and software-defined radio, and radar architectures for telecommunications, remote sensing, and biomedical applications.

Dr. Gómez-García is a member of the IEEE MTT-S Microwave Acoustics (MTT-2), the IEEE MTT-S Filters and Passive Components (MTT-8), the IEEE MTT-S Biological Effects and Medical Applications of RF and Microwave (MTT-10), the IEEE MTT-S Wireless Communications (MTT-20), and the IEEE CAS-S Analog Signal Processing Technical Committees. He also serves as a member for the Technical Review Board for several IEEE and EuMA conferences. He was a recipient of the 2016 IEEE Microwave Theory and Techniques Society (MTT-S) Outstanding Young Engineer Award. He was an Associate Editor of the IEEE TRANSACTIONS ON CIRCUITS AND SYSTEMS—I:REGULAR PAPERS from 2012 to 2015 and the IEEE TRANSACTIONS ON MICROWAVE THEORY AND TECHNIQUES from 2012 to 2016. He was a Guest Editor of the 2013 IEEE JOUR-NAL ON EMERGING AND SELECTED TOPIS IN CIRCUITS AND SYSTEMS "Special Issue on Advanced Circuits and Systems for CR/SDR Applications," the IET Microwaves, Antennas, and Propagation 2013 "Special Issue on Advanced Tunable/Reconfigurable and Multi-Function RF/Microwave Filtering Devices," and the IEEE Microwave Magazine 2014 "Special Issue on Recent Trends on RF/Microwave Tunable Filter Design." He is currently an Associate Editor of the IEEE JOURNAL OF ELECTROMAGNETICS, RF AND MICROWAVES IN MEDICINE AND BIOLOGY, IEEE ACCESS, and IET Microwaves, Antennas, and Propagation. He is a Senior Editor of the IEEE JOURNAL ON EMERGING AND SELECTED TOPICS IN CIRCUITS AND SYSTEMS. He is also a Reviewer for several IEEE, IET, EuMA, and Wiley



**José-María Muñoz-Ferreras** (M'15) was born in Madrid, Spain, in 1981. He received the degree in telecommunication engineering and the Ph.D. degree in electrical and electronic engineering from the Polytechnic University of Madrid, Madrid, in 2004 and 2008, respectively.

He is currently an Associate Professor with the Department of Signal Theory and Communications, University of Alcalá, Alcalá de Henares, Spain. His current research interests include radar signal processing, advanced radar systems and concepts,

and microwave/RF circuits and systems, specifically focusing on high-resolution inverse synthetic aperture radar images and the design and validation of radar systems for short-range applications.

Dr. Muñoz-Ferreras is a member of the IEEE MTT-S Biological Effects and Medical Applications of RF and Microwave (MTT-10) Technical Committee. He also serves as a member of the Technical Review Board of the IEEE International Geoscience and Remote Sensing Symposium, the IEEE Radar Conference, and the European Radar Conference. He is a Reviewer for several IEEE and IET publications.



**Dimitra Psychogiou** (S'10–M'14) received the Dipl.-Eng. degree in electrical and computer engineering from the University of Patras, Patras, Greece, in 2008, and the Ph.D. degree in electrical engineering from the Swiss Federal Institute of Technology, Zürich, Switzerland, in 2013.

She was a Research Scientist with Purdue University, West Lafayette, IN, USA, from 2013 to 2016. She is currently an Assistant Professor of electrical, computer and energy engineering with the University of Colorado Boulder, Boulder, CO, USA.

Her current research interests include RF design and characterization of reconfigurable microwave and millimeter-wave passive components, RF-MEMS, acoustic wave resonator-based filters, tunable filter synthesis, and frequency-agile antennas.

Dr. Psychogiou is a member of the IEEE MTT-S Filters and Passive Components (MTT-8) Committee and the IEEE MTT-S Microwave Control Materials and Devices (MTT-13) Technical Committee. She is currently an Associate Editor of IEEE MICROWAVE AND WIRELESS COMPONENTS LETTERS and *IET Microwaves, Antennas, and Propagation*. She serves on the Technical Review Board for various IEEE and EuMA conferences and journals.